



Co-funded by  
the European Union

# EXSOLUTION-BASED NANOPARTICLES FOR LOWEST COST GREEN HYDROGEN VIA ELECTROLYSIS



## Candidate electrode exsolved material selection integrated Deliverable D1.1

The project is supported by the Clean Hydrogen Partnership and its members		
PU	Public, fully open	<input checked="" type="checkbox"/>
SEN	Sensitive, limited under the conditions of the Grant Agreement	<input type="checkbox"/>
Classified R-UE/EU-R	EU RESTRICTED under the Commission Decision No2015/444	<input type="checkbox"/>
Classified C-UE/EU-C	EU CONFIDENTIAL under the Commission Decision No2015/444	<input type="checkbox"/>
Classified S-UE/EU-S	EU SECRET under the Commission Decision No2015/444	<input type="checkbox"/>

*Co-funded by the European Union. Views and opinions expressed are however those of the author(s) only and do not necessarily reflect those of the European Union or Clean Hydrogen JU. Neither the European Union nor the granting authority can be held responsible for them.*

---

## NOTICES

---

For information, please contact the project coordinator, Elo Meier, e-mail: [elo.meier@stargatehydrogen.com](mailto:elo.meier@stargatehydrogen.com). This document is intended to fulfil the contractual obligations of the EXSOTHyC project, which has received funding from the Clean Hydrogen Partnership and its members, concerning deliverable D1.1 described in contract 101137604.

All intellectual property rights are owned by EXSOTHyC consortium and are protected by the applicable laws. Except where otherwise specified, all document contents are: “©EXSOTHyC Project - All rights reserved”.

Reproduction is not authorized without prior written agreement. The commercial use of any information contained in this document may require a license from the owner of that information. EXSOTHyC consortium is also committed to publish accurate and up to date information and take the greatest care to do so. However, EXSOTHyC consortium cannot accept liability for any inaccuracies or omissions nor accept liability for any direct, indirect, special, consequential, or other losses or damages of any kind arising out of the use of this information.

---

## Authors

---

Evangelos Andreou, Cristian Savaniu, John Irvine (St Andrews)

---

## Reviewer(s)

---

Nadine Eißmann, Felix Neupert, Stefan Loos (IFAM)

---

## Table of revisions

---

Version	Date	Description and reason	Author	Affected sections
V0.1	20/04/26	Draft	Evangelos Andreou, Cristian Savaniu, John Irvine	All
...	27/04/26	Proofreading	Nadine Eißmann, Stefan Loos, Felix Neupert	All
V1.0	30/04/26	Final	Evangelos Andreou	-



---

## List of Partners

---

Stargate Hydrogen Solutions OÜ (Stargate)  
University of St Andrews (St Andrews)  
Agfa-Gevaert NV (AGFA)  
Eindhoven University of Technology (TUE)  
Fraunhofer IFAM (IFAM)

---

## List of Abbreviations

---

AWE: Alkaline Water Electrolyzer

LCTCo:  $\text{La}_{0.42}\text{Ca}_{0.48}\text{Ti}_{0.89}\text{Co}_{0.11}\text{O}_3$

LCTNiFe:  $\text{La}_{0.43}\text{Ca}_{0.37}\text{Ti}_{0.94}\text{Ni}_{0.03}\text{Fe}_{0.03}\text{O}_3$

p-XRD: Powder X-ray Diffraction

STEM: Scanning Transmission Electron Microscopy

HER: Hydrogen Evolution Reaction

OER: Oxygen Evolution Reaction

LSV: Linear Sweep Voltammetry

RDE: Rotating Disk Electrode

---

## List of Figures

---

Figure 1. XRD patterns of LCTCo and LCTNiFe synthesized materials.

Figure 2. Representative nitrogen physisorption isotherms of LCTCo material.

Figure 3. A) Representative TEM image of R-LCTCo material. B) EDS profile of the exsolved nanoparticle.

Figure 4. Representative TEM image and elemental profile of R-LCTNiFe material.

Figure 5. iR-compensated LSV curves of perovskite materials for A) HER and B) OER

Figure 6. Representative XRD patterns of LCTCo materials after calcination (C-LCTCo), reduction (R-LCTCo) and phosphidation (P-LCTCo).

Figure 7. TEM image (a) and elemental profile (b) of P-LCTCo electrocatalyst.

Figure 8. iR-compensated LSV curves of perovskite materials for A) HER and B) OER

Figure 9. Polarization of zero-gap single cell arrangements with plain cathode and Zirfon Perl diaphragm.

## Table of Contents

---

NOTICES.....	2
Authors .....	3
Reviewer(s) .....	3
Table of revisions.....	3
List of Partners .....	4
List of Abbreviations .....	5
List of Figures .....	5
1 Objectives.....	7
2 Work done .....	7
2.1 Exsolved Catalyst selection- Experimental Results .....	7
3 Deviations.....	15
4 Conclusions.....	15
5 List of References.....	16

## 1 Objectives

The objective of this deliverable is to summarize the process of developing exsolved electrode materials that will be integrated with nickel foam substrates for alkaline water electrolyzer (AWE) performance assessment. The focus of this activity is to develop exsolution candidate electrocatalysts that exhibit high electrochemical activity and stability for both HER and OER under alkaline conditions. Then, based upon the experimental data, the material selection has been made and complete integration of the material into the conductive nickel foam substrate will follow.

## 2 Work done

### 2.1 Exsolved Catalyst selection - Experimental Results

St Andrews has optimized a spray drying process to produce a large scale (>200 g) of perovskite oxide materials. We developed several candidate materials, but, after selection, only the two most promising will be discussed, namely: i)  $\text{La}_{0.42}\text{Ca}_{0.48}\text{Ti}_{0.89}\text{Co}_{0.11}\text{O}_3$  (LCTCo) and ii)  $\text{La}_{0.43}\text{Ca}_{0.37}\text{Ti}_{0.94}\text{Ni}_{0.03}\text{Fe}_{0.03}\text{O}_3$  (LCTNiFe).

#### Powder Preparation

The above perovskite oxide powders were obtained by a precursor solution spray drying technique. Specifically, an aqueous metal precursor solution (0.5 M/l) was prepared by dissolving appropriate amounts of  $\text{La}(\text{NO}_3)_3 \cdot 6\text{H}_2\text{O}$ ,  $\text{Ca}(\text{NO}_3)_2 \cdot 4\text{H}_2\text{O}$ , Ti(IV) bis(ammonium lactate) dihydroxide ( $\text{TiC}_6\text{H}_{18}\text{N}_2\text{O}_8$ ) and  $\text{Co}(\text{NO}_3)_2 \cdot 6\text{H}_2\text{O}$  or  $\text{Ni}(\text{NO}_3)_2 \cdot 6\text{H}_2\text{O}$  and  $\text{Fe}(\text{NO}_3)_3 \cdot 9\text{H}_2\text{O}$ . Then, stoichiometric amount of citric acid (1:1 mole ratio to the total metal ions) is added to the solution and left under vigorous stirring for one hour. After the dissolution of citric acid, the pH of the solution was adjusted to 7 by the addition of  $\text{NH}_4\text{OH}$  (25 % wt.) and the solution was left under stirring for 1 hour. The resulting solution was then transferred through a nylon line and a peristaltic pump into a SD06 unit (Lab Plant) and sprayed, as the solvent evaporation occurred at  $250^\circ\text{C}$ . Afterwards, the resulting recovered fine powders were calcined at  $900^\circ\text{C}$  for two hours at  $3^\circ\text{C min}^{-1}$  ramp rate. The calcined materials are denoted as C-LCTCo or C-LCTNiFe.

The exsolution of the metallic nanoparticles was performed in a tubular furnace under reducing atmosphere. In particular, 100 mg of the calcined catalyst was inserted into a tube furnace and was heated at  $800^\circ\text{C}$  with a ramp rate of  $5^\circ\text{C min}^{-1}$  under 5%  $\text{N}_2/\text{H}_2$  saturated atmosphere for 2 hours to obtain the R-LCTCo or R-LCTNiFe catalyst, respectively.

#### Physicochemical and morphological Characterization

All materials were characterized by powder X-ray diffraction measurements to determine the purity of the powder and crystalline properties. Fig. 1 depicts the p-XRD pattern of the LCTCo and LCTNiFe materials. The results confirm that we have successfully obtained the pure phase of the perovskite oxide electrocatalyst.

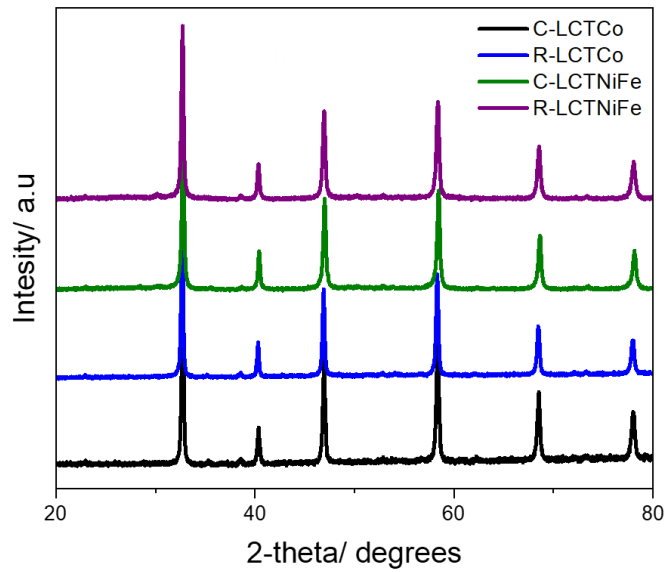


Figure 1. XRD patterns of LCTCo and LCTNiFe, as prepared (C) and reduced materials (R).

The diffraction peaks of LCTCo correspond to a perovskite structure of orthorhombic (Pbnm) symmetry, with unit cell parameters  $a = 5.4709(3) \text{ \AA}$ ,  $b = 5.4718(7) \text{ \AA}$ , and  $c = 7.7373(5) \text{ \AA}$ ; the unit cell parameters of the reduced sample, R-LCTCo, are larger than the ones of the calcined one, due to larger size of  $\text{Ti}^{3+}$  ( $0.67 \text{ \AA}$ ) obtained by reduction, compared to the initial  $\text{Ti}^{4+}$  ( $0.605 \text{ \AA}$ ) ( $a = 5.4727(3) \text{ \AA}$ ,  $b = 5.4738(5) \text{ \AA}$ , and  $c = 7.7432(4) \text{ \AA}$ ).

The porosity of the materials upon calcination at  $800 \text{ }^\circ\text{C}$  was examined by  $\text{N}_2$  physisorption measurements. The isotherms depicted in Fig. 2, correspond to a type-III curve accompanied with an H3-type hysteresis loop, which is characteristic for macroporous or non-porous materials with slit-shaped pores; with The Brunauer-Emmet-Teller (BET) specific surface areas range from  $6$  to  $10 \text{ m}^2 \text{ g}^{-1}$  and the relative pore volumes from  $0.002 \text{ cm}^3 \text{ g}^{-1}$  to  $0.063 \text{ cm}^3 \text{ g}^{-1}$ , respectively. In terms of particle size, after milling at  $500 \text{ rpm}$  for two h, the calcined powder containing soft agglomerates, the size decreases to  $d_{50} \sim 1.8 \text{ }\mu\text{m}$ , that is suitable for dispersion preparation for Ni foam coating.

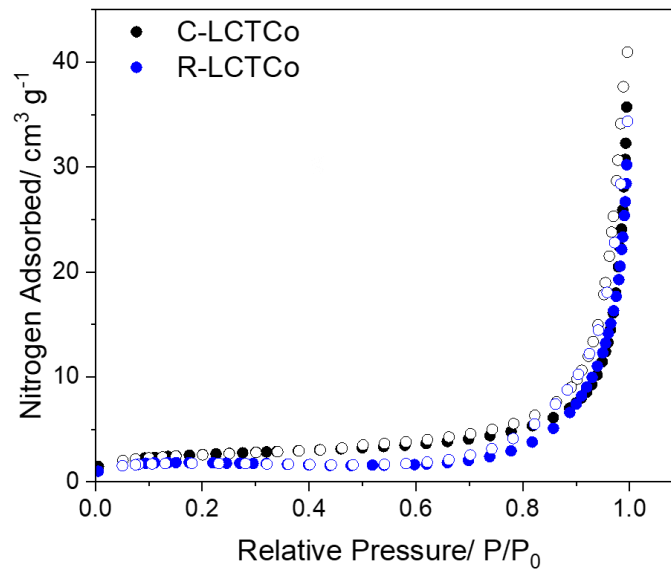


Figure 2. Representative nitrogen physisorption isotherms of LCTCo material.

Then, we proceeded to examine the exsolution process of the candidate materials upon reduction via Scanning Transmission Electron Microscopy (STEM). Fig. 3 and 4 display the high-resolution TEM and EDS profile of LCTCo and LCTNiFe electrocatalysts. After reduction treatment, the exsolution of metallic Co and NiFe nanoparticles of around  $\sim 25$  nm can be observed. Taking a more thorough look into the reduced R-LCTCo material, Fig. 3 and 4 depict the representative TEM images, in which we can clearly observe the exsolution of Co and NiFe nanoparticles of  $\sim 25$  nm. EDS profile on the exsolved Co nanoparticle, provides further evidence for successful exsolution on titanate-based perovskite. As can be seen in Fig. 3 and 4, the absence of intensity of the other elements except Co across the particle region, strongly confirms that Co and NiFe nanoparticles have been exsolved.

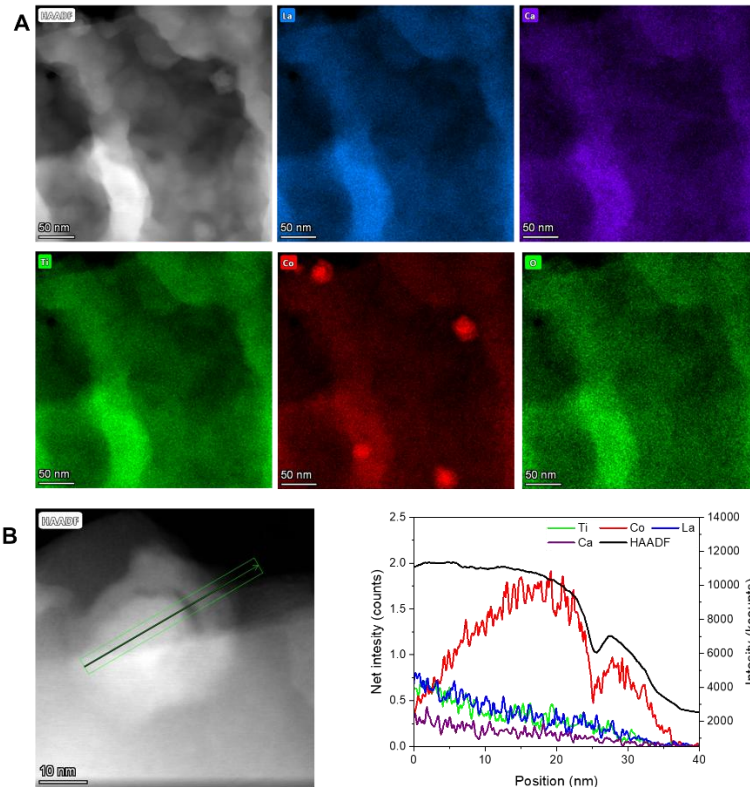


Figure 3. A) Representative TEM image of R-LCTCo material. B) EDS profile of the exsolved nanoparticle.

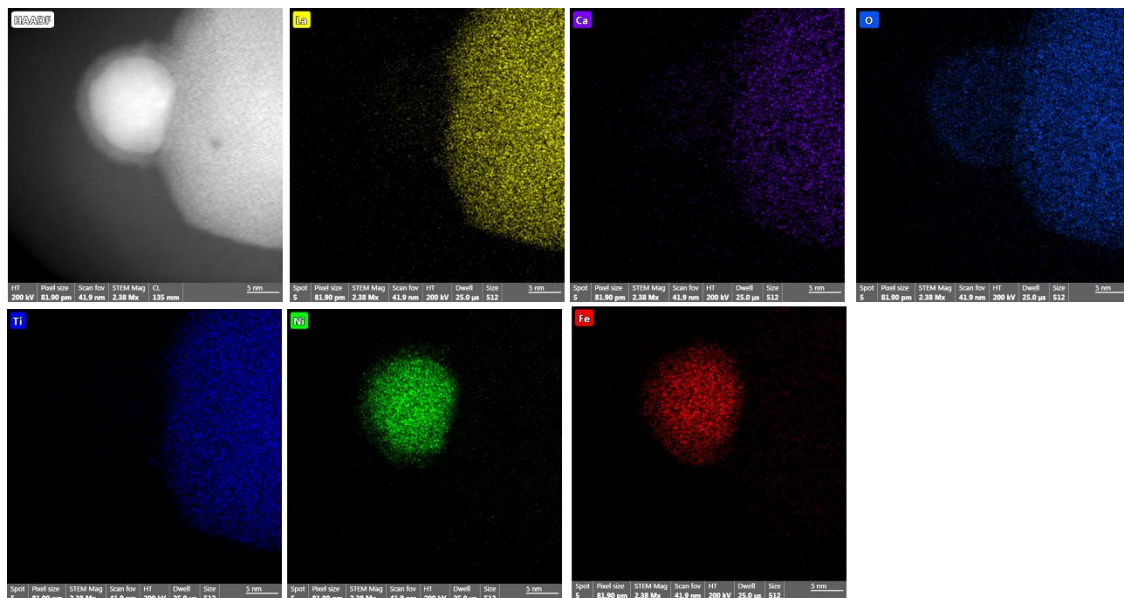


Figure 4. Representative TEM image and elemental profile of R-LCTNiFe material.

### Electrocatalytic activity of the perovskite oxides

The electrocatalytic performance of the as-prepared catalysts (drop-casted on a glassy carbon working electrode) was assessed under alkaline conditions (1 M KOH) in a typical three-electrode electrochemical workstation. Fig. 5 depicts the iR-corrected linear sweep

voltammogram (LSV) curves for the LCTCo and LCTNiFe catalysts used to assess the electrocatalytic activity towards the hydrogen and oxygen evolution reaction (HER & OER). We also synthesized an undoped LCT material for comparison purposes. In particular, pristine LCT materials exhibit a poor electrocatalytic performance for HER, yielding an overpotential at  $10 \text{ mA cm}^{-2}$  of 515 mV. Upon introduction of cobalt in the crystal lattice of the perovskite and reduction the electrocatalytic performance is enhanced (C-LCTCo & R-LCTCo), displays an overpotential of 440 mV at  $10 \text{ mA cm}^{-2}$ . Interestingly, the exsolution of metallic cobalt nanoparticles on the surface of the perovskite does not affect the activity towards HER, suggesting that cobalt nanoparticles do not display high catalytic activity for hydrogen production. However, OER performance the calcined material exhibited an overpotential of 510 mV at  $10 \text{ mA cm}^{-2}$  and the reduced material a 490 mV overpotential at same current density.

As observed, for HER, the calcined LCTNiFe material exhibited an overpotential of 430 mV at  $10 \text{ mA cm}^{-2}$  and the R-LCTNiFe 385 mV. For OER, the calcined material exhibited an overpotential of 460 mV at  $10 \text{ mA cm}^{-2}$  and the reduced material 390 mV, respectively.

Although the exsolved powders exhibited good electrocatalytic activities towards water splitting reaction, it was still desirable to further improve them in order to be successfully integrated to nickel foam electrodes for AWE systems. So, we then proceeded on implementing advanced synthetic methods to further improve the electrocatalytic performance of the modified material.

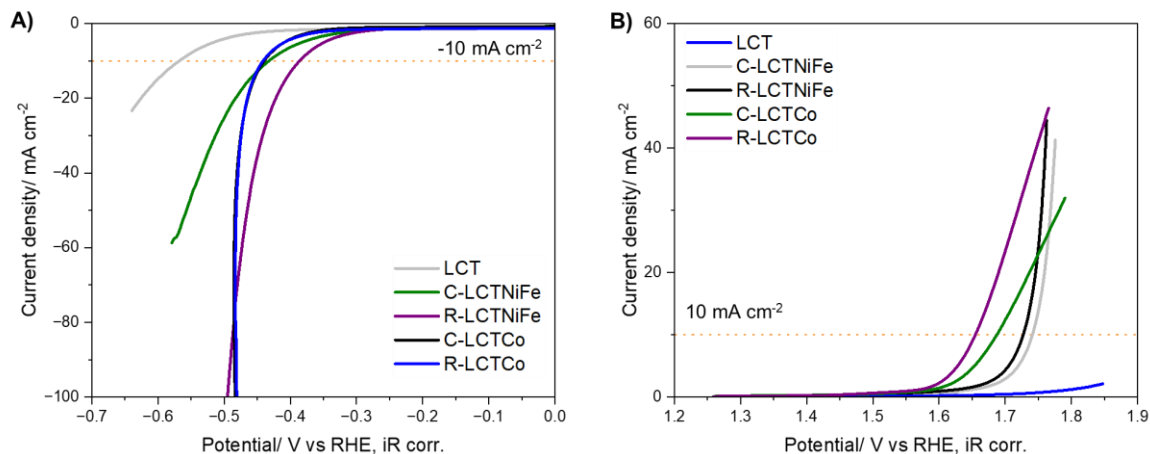


Figure 5. iR-compensated LSV curves of perovskite materials for A) HER and B) OER

### Phosphorus surface functionalization of the exsolved nanoparticles.

Due to the fact that the exsolved nanoparticles are solely metallic, that results in limited electrocatalytic activity. So, we proceeded to functionalizing the exsolved nanoparticles with phosphorus in order to yield the highly active transition metal phosphides catalytic species. This method, consisting in exposure of reduced sample to a phosphorus gaseous source ( $\text{PH}_3$ ) at  $400 \text{ }^\circ\text{C}$ , provides the opportunity of devising exsolved nanoparticles

possessing the durability of the anchored nature from exsolution process, and the redox kinetics/activity of the transition metal phosphides [1-2].

The XRD of the phosphorus decorated exsolved nanoparticles, did not show any additional diffraction peaks; indicating the formation of CoP and NiFeP amorphous nanoparticles on the surface of the perovskite oxide (Fig.6). The lack of detection of corresponding diffraction peaks for CoP and NiFeP is due to the small size of exsolved, modified nanoparticles.

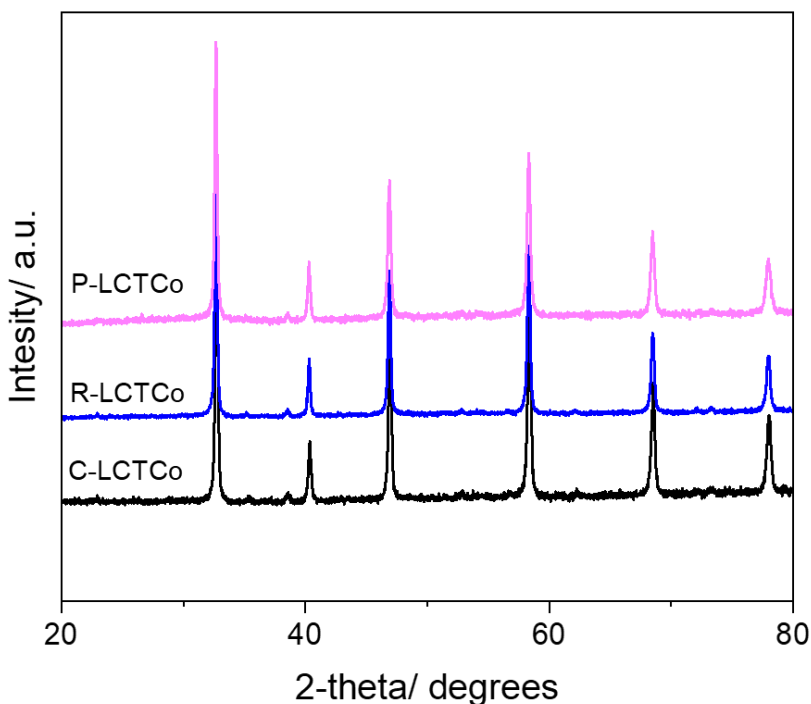


Figure 6. Representative XRD patterns of LCTCo materials after calcination (C-LCTCo), reduction (R-LCTCo) and phosphidation (P-LCTCo).

We then proceeded to characterizing the modified materials via STEM. Compared to XRD, a more detailed look of the phosphidation process came from STEM imaging. Fig. 7 shows the representative TEM images of P-LCTCo, showing the presence of exsolved Co of  $\sim 50$  nm size. After phosphidation, the exsolved Co particles have been fully covered by phosphorus atoms, thus creating the CoP catalytic active site. The larger size of the exsolved particles in the P-LCTCo and P-LCTNiFe in regard to the reduced material, can be related due to the high reductive behaviour of  $\text{PH}_3$ , which can further enhance the exsolution of metallic nanoparticles or subjecting the already exsolved sample to a second high temperature treatment required for phosphidation. The EDS profile in both materials, further indicates the successful synthesis of exsolved CoP and NiFe catalytic active sites for water electrolysis.

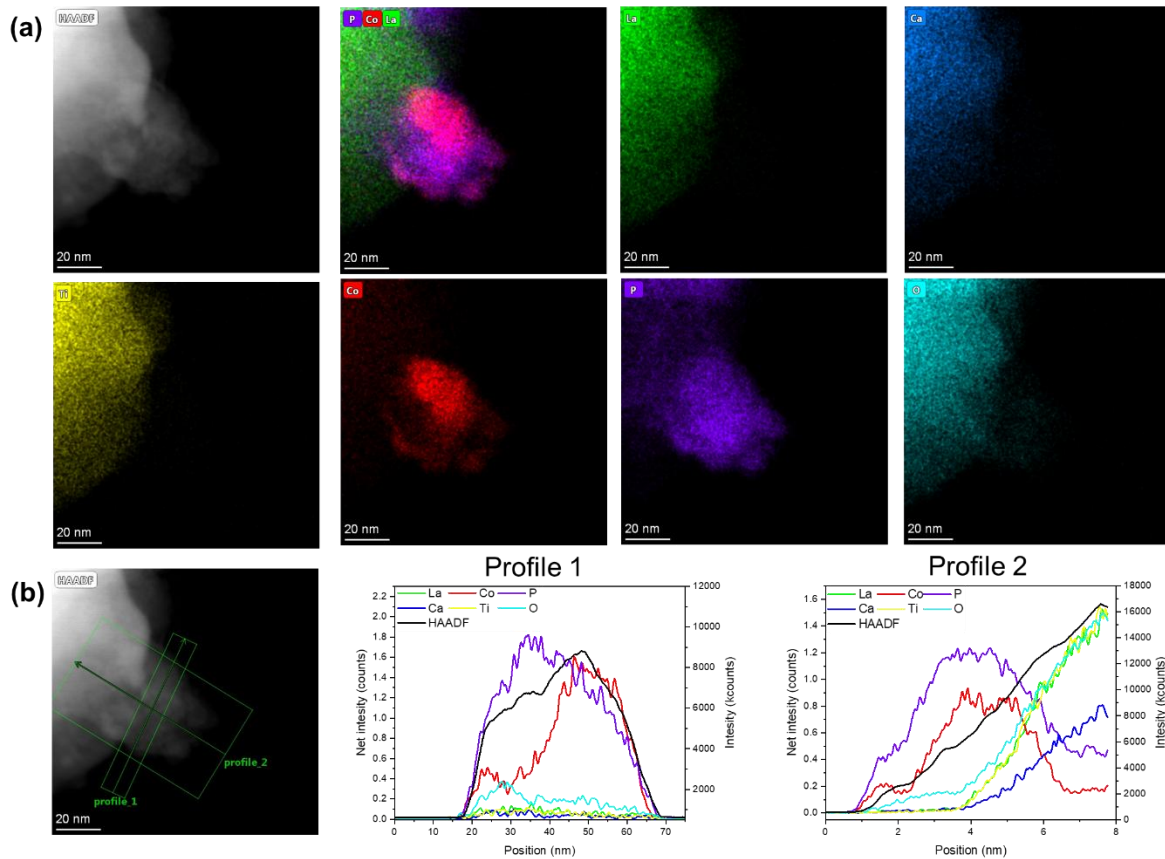


Figure 7. TEM image (a) and elemental profile (b) of P-LCTCo electrocatalyst.

To examine the effect of the phosphorus functionalization experiments (1M KOH, RT) in three-electrode set-up, using a RDE were conducted. Fig. 8, displays the HER and OER catalytic activity of the modified material. The results suggest that the phosphorus functionalization plays a crucial role on enhancing the redox properties of the materials. Specifically, the P-LCTCo exhibit overpotential at 10 mA cm<sup>-2</sup> for HER (287 mV) and OER (390 mV), while the P-LCTNiFe, displayed overpotentials of 330 mV for HER and 390 mV for OER upon phosphidation treatment. These activities were higher than the reduced materials, where higher overpotentials have been obtained (R-LCTCo: HER: 440 mV & OER: 440 mV, R-LCTNiFe: HER: 385 mV & OER: 390 mV).

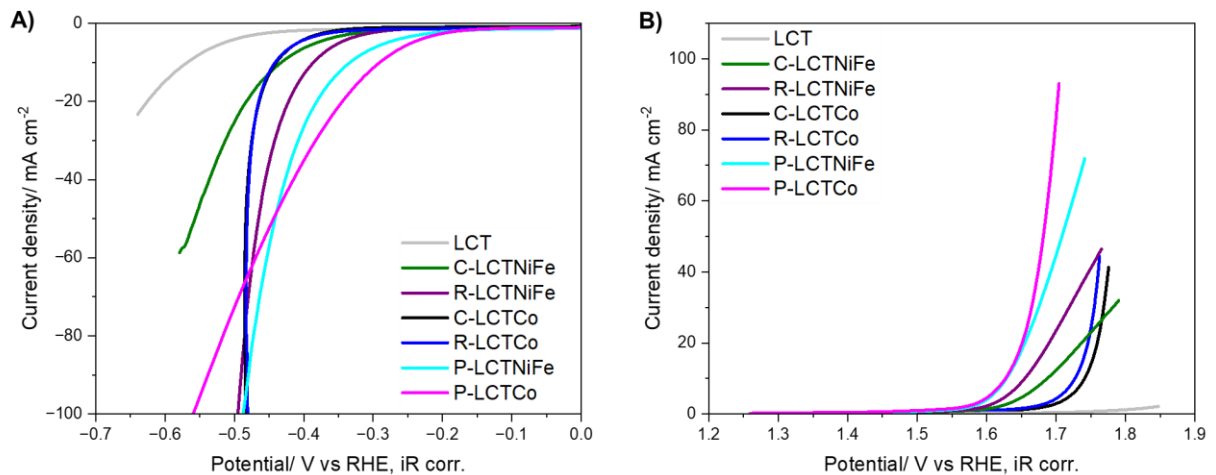


Figure 8. iR-compensated LSV curves of perovskite materials for A) HER and B) OER

In general, the phosphidation of the exsolved nanoparticles showed promising results in terms of enhancing the electrocatalytic activity of the material. Also, we identified an additional method of boosting the catalytic activity by deposition of co-catalysts (metal oxides, metal oxohydroxides etc.) and the optimisation of synthesis conditions and electrochemical testing are under way.

Regarding, the selection of the perovskite oxide to integrate onto the Ni foams substrates, we chose the LCTCo catalyst, although, the LCTNiFe exhibits a marginally better performance on RDE measurements than LCTCo. When tested in relevant conditions, in AWE single cell, under 30 wt. % KOH, at 80 °C, the LCTCo catalyst was found, in fact, to have a better performance (Figure 9).

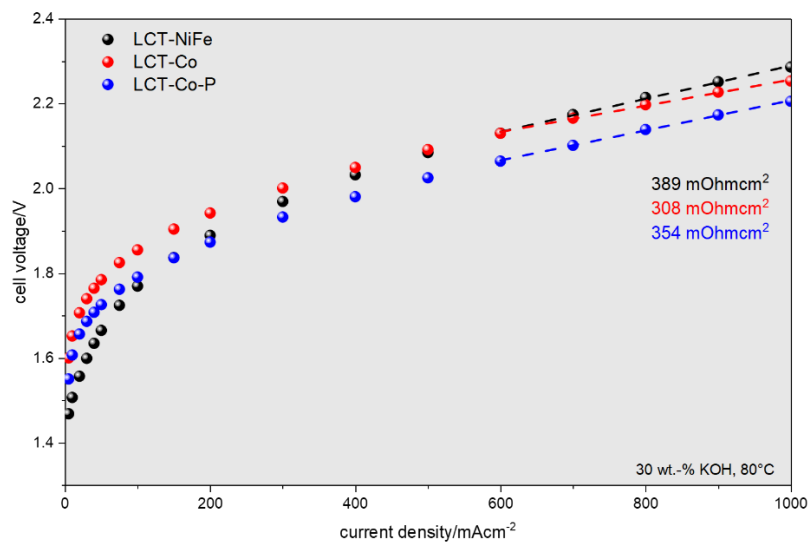


Figure 9: Polarization of zero-gap single cell arrangements with plain cathode and Zirfon Perl diaphragm.

LCT-NiFe exhibits the largest intrinsic activity, LCT-Co outperforms the NiFe-version at elevated currents, as it shows improved conductivity. Phosphidation has further improved the LCTC-Co system and changes the nature of the Co-nanoparticles towards higher OER-activity.

Although Co is considered a critical and strategic raw material in the EU, its level in this composition (3.7 wt% or 0.15 mg Co/cm<sup>2</sup> electrode) is below the accepted threshold in the Project, i.e. <0.3 mg/W.

---

### 3 Deviations

---

While the phosphidation route was very promising as can be seen above, for the final selection of electrode this will not be implemented due to difficulty in electrode scaling up. We will examine the AWE performance of the LCTCo material in order to have a full investigation of the exsolved nanoparticles under those conditions for the first time. The second option of functionalisation, i.e. the addition of co-catalysts is more suitable for scaling up.

---

### 4 Conclusions

---

We have successfully developed perovskite oxide electrode candidates for integration on the nickel foam substrates. We have also identified new synthetic routes of further enhancing the electrocatalytic activity of those materials such as phosphidation and deposition of co-catalysts. Taking into consideration our results, we will integrate the LCTCo catalyst onto Ni foams substrates to be tested in the AWE stack.

---

## 5 List of References

---

- 1) Neagu, D.; *et al.* Perovskite oxide electrodes for protonic ceramic electrochemical cells. *J. Phys. Energy* **2023**, *5*, 031501. <https://doi.org/10.1088/2515-7655/acd146>.
- 2) Pu, Z.; *et al.* Transition-Metal Phosphides: Activity Origin, Energy-Related Electrocatalysis Applications, and Synthetic Strategies. *Adv. Funct. Mater.* **2020**, *30*, 2004009. <https://doi.org/10.1002/adfm.202004009>.